Research Article | Vol. 15, No. 5 / 1 May 2025 / Optical Materials Express 1005

Optical Materials EXPRESS

Effect of substrate and beam diameter on direct laser patterning of ruthenium thin films

Lorenzo Cruciani,[1,2,*] Marnix Vreugdenhil,[3] Dries van Oosten,[3] Klaasjan van Druten,[2] and Paul Planken[1,2]

[1]Advanced Research Center for Nanolithography, Science Park 106, 1098 XG, Amsterdam, The Netherlands
[2]Van der Waals-Zeeman Institute, Institute of Physics, University of Amsterdam, Science Park 904, 1098 XH Amsterdam, The Netherlands
[3]Debye Institute for Nanomaterials Science and Center for Extreme Matter and Emergent Phenomena, Utrecht University, Princetonplein 5, 3584 CC Utrecht, The Netherlands
[*]cruciani@arcnl.nl

Abstract: Recently, a method was introduced to produce ruthenium/ruthenium-oxide electrically conductive islands through laser-induced oxidation of ruthenium thin films, followed by subsequent removal of the un-oxidized ruthenium using a NaClO solution. In this paper, we provide additional insight intp the patterning process by measuring the effect of Ru film thickness and substrate material on the pattern formation. In particular, understanding the role of the substrate, which affects the island formation mainly through the Ru film-substrate interfacial thermal conductance, is crucial. Experimental results and numerical heat diffusion calculations are used for comparing the island formation process when using a 2 μm exposure beam diameter and a 0.8 μm one. It is shown that in-plane heat diffusion results in a faster decay of the surface lattice temperature of the film after exposure to the 0.8 μm beam diameter. Although exposing the samples to a smaller beam diameter could, in principle, enable obtaining patterns with smaller features, in-plane heat diffusion may be the limiting factor for the smallest features achievable using this method.

1. Introduction

In recent years, novel materials have been investigated with the goal of improving the performance of semiconductor devices [1,2]. Among these, ruthenium has raised interest due to its relatively high nanoscale electrical conductivity resulting from the small grain sizes [3,4]. In addition, Ru and RuO_2 are suitable for applications in semiconductor manufacturing thanks to their chemical and thermal stability [5–7], both of which are beneficial for the lifetime and the performance of devices. Ruthenium being a relatively unknown material, it is worth pointing out a number of interesting properties, such as the high melting point of Ru (2 583 K), and the fact that the oxide RuO_2 has a low resistivity of 35 $\mu\Omega$ cm [8].

Recently we described a method for patterning Ru based on laser-induced oxidation of Ru thin films [9]. In short, exposure to femtosecond (fs) laser pulses results in a temperature increase of the Ru film. When the temperature exceeds a certain threshold, a less than 2 nm thick layer near the surface of the film is partially oxidized. By focusing a beam with a gaussian spatial profile and by tuning the exposure fluence, repetition rate and exposure time, it is possible to limit oxidation to the most central region of the beam. The un-exposed Ru is dissolved using a NaClO solution, while the top layer of RuO_2 prevents dissolution of the exposed region, such that the Ru pattern with a thin conductive RuO_2 top layer remains. Using a fs pulsed exposure laser with a 1030 nm wavelength, focused to a spot with a 2 μm diameter this method allowed us to obtain islands with a diameter of approximately 500 nm: four times smaller than the beam diameter and therefore below the optical diffraction limit of the system used for illumination.

Here, we further explore our patterning method with the aim of providing additional insight into its applicability. We explore the effect of Ru film thickness, correlating it with the exposure

#559351 https://doi.org/10.1364/OME.559351
Journal © 2025 Received 14 Feb 2025; revised 4 Apr 2025; accepted 5 Apr 2025; published 17 Apr 2025

Optical Materials EXPRESS

fluences necessary to produce the patterns. We calculate the absorption of Ru as a function of the film thickness, which shows a weak dependence for thicknesses above approximately 8 nm. We find that the threshold fluence necessary to produce Ru/RuO_2 islands from 20 nm and 50 nm thick films, scales with the film thickness. This suggests that the fluence needed for applying this method to different film thicknesses may simply be predicted from the film thickness, as long as the film is homogeneously heated over its thickness.

The role of the substrate material underneath the Ru is studied by comparing the island formation process on three different substrates: glass, sapphire and silicon. We extract similar threshold fluences for sapphire and silicon, regardless of their different thermal conductivities. This suggests that the Ru/substrate interfacial thermal conductances (ITC) for the three substrate materials play a crucial role in slowing down heat transport into the substrates.

Results obtained with different exposure beam diameters are compared both by measuring the island-formation threshold fluence as a function of the number of pulses used for exposure and by numerical simulations of heat diffusion. This shows that, after exposure to a 0.8 μm beam diameter, in-plane heat transport results in a faster decay of the lattice surface temperature, compared to exposure to a 2 μm diameter beam. While in principle the possibility to produce patterns by means of a smaller exposure diameter would make it possible to obtain features with smaller dimension, in-plane heat transport may be the limiting factor determining the minimum achievable feature size.

2. Materials and methods

Ruthenium thin films were deposited via magnetron sputtering at an argon plasma pressure of 2×10^{-3} mbar. We extracted the deposition rate of the magnetron sputterer by depositing thick Ru layers (> 100 nm) and measuring their thickness using a contact profilometer. We then extracted a calibration curve consisting of Ru film thickness versus deposition time. From this, we measured a deposition rate of 0.25 nm/s. The film thickness was then chosen by setting the deposition time according to this rate. Glass, silicon and sapphire were used as substrates. The substrates were chemically cleaned using a solution of ammonium hydroxide (NH_4OH) with hydrogen peroxide in water and, subsequently, rinsed in isopropanol.

A schematic of the setup used for laser exposure is shown in Fig. 1. The laser has a 1030 nm wavelength and delivers pulses with a duration of approximately 200 fs with a 200 kHz repetition rate. The laser was chosen because it offers a tunable repetition rate and because it has the ability to vary the number of laser shots. In addition, the sub-picosecond-duration of the laser pulses is shorter than the timescale at which the lattice heats up. This simplifies the interpretation of the experimental results and the numerical calculations. A half-wave plate and a polarizing beam splitter (PBS) are used to control the exposure fluence. We note that, throughout this paper, we report the single-pulse fluence even when referring to exposure to multiple pulses. A reflective spatial light modulator (SLM, Santec SLM-300) is used to control the diameter of the beam. This is done by forming a blazed grating within a circular area on the SLM. This grating effectively acts as an aperture, as only the light that hits the grating show a first order diffraction. By changing this *effective-aperture* diameter, the diameter of the first-order diffracted beam is varied. The diffracted beam is then directed to a microscope objective, which focuses it onto the sample. The beam diameter at the focus of the objective can be continuously varied between 2 μm and 0.8 μm by varying the diameter of the effective aperture of the spatial light modulator. When the aperture is fully open, the diameter of the first-order-diffracted beam is largest and it illuminates the full entrance of the objective, resulting in the smallest focal diameter of 0.8 μm. Decreasing the effective aperture diameter reduces the diameter of the diffracted beam, which results in an increased focal spot diameter. The beam diameter and shape were extracted from an image of the beam reflected from a mirror placed at the focus of the microscope objective. The diameter was extracted by performing a gaussian fit to the image of the beam.

Optical Materials EXPRESS

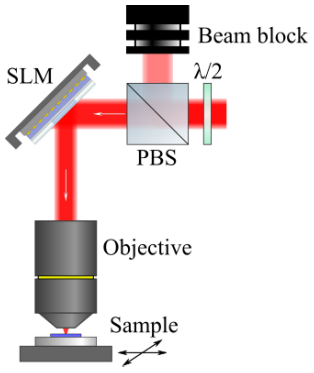

Fig. 1. Schematics of the laser-exposure setup used for producing the laser-induced oxidation with variable beam diameter before immersion in the NaClO solution [10]. PBS: polarizing beam splittes; SLM: spatial light modulator.

After exposure, the samples were immersed in a 3-7% NaClO solution in water, which dissolves the un-exposed Ru and leaves only the partially oxidized areas on the substrates. After this, the samples were rinsed in demineralized water and, subsequently, in isopropanol.

The Ru/RuO_2 island formation process is studied by measuring the area of the islands remaining after the aforementioned fabrication procedure, using an optical microscope. We then plot the area of the islands as a function of the logarithm of the exposure fluence of the beam. When this so called Liu plot [11] is linear, it is possible to extract the (single-pulse) threshold fluence for island formation by performing a linear fit to the data and, from this, extracting the fluence value at which the area is zero. An alternative method, allowing to extract high-repetition-rate laser fluence thresholds, is described in [12].

3. Results

To gain more insight into the effect of Ru layer thickness on the amount of absorbed light, we calculated the percentages of absorbed, transmitted and reflected light as a function of the Ru film thickness on glass. The calculations were performed by assuming light orthogonally incident on the sample, and using the complex refractive index $\tilde{n} = n + ik$ of Ru obtained earlier using ellipsometry, namely $\tilde{n} = 4.925 + i5.010$, obtained at 1 000 nm, the longest wavelength accessible in the ellipsometer. The ellipsometry measurements are similar to those reported in [13]. For glass, we used a refractive index of 1.5. The results are shown in Fig. 2. The percentages of reflected and transmitted light approach the bulk values for thicknesses above approximately 60 nm (69% and ~0% in the figure, respectively). The amount of absorbed light (black solid line) has a maximum of 40% for a Ru thickness of 8 nm, after which it slightly decreases to a value of 29% at a thickness of approximately 40 nm and increases again until reaching the bulk value of 33% around 80 nm. Below, we will show results of experiments performed on Ru layers having a thickness of 20 and 50 nm. Ruthenium shows an insulator-to-metal transition from thicknesses above approximately 10 nm [14]. For this reason, and from an application perspective, we chose thicknesses well above this limit.

From Fig. 2 we can see that for the 20 nm thick sample, the expected percentage of absorbed light is 34 %, whereas for the 50 nm thick layer it is about 30%. The same calculations resulting in Fig. 2 were performed for Ru on sapphire and for Ru on silicon. The refractive index of the substrates used in the calculations was 1.7557 for sapphire and $3.5757 + i4902 \times 10^{-4}$ for silicon. For both substrates, the calculations do not show large variations in the amount of absorbed light for Ru film thickness above ~10 nm.

Optical Materials EXPRESS

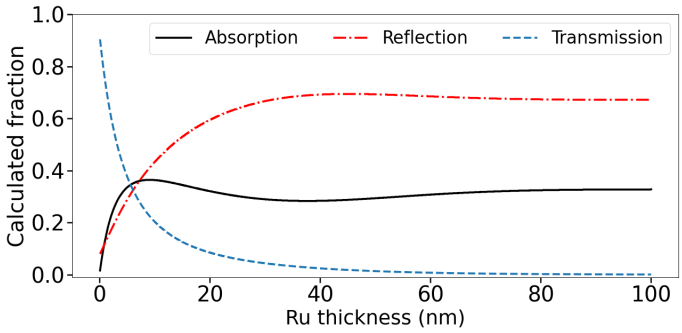

Fig. 2. Calculated amounts of absorbed (black, solid line), reflected (red, dashed-dotted) and transmitted (blue, dashed) light with a wavelength of 1000 nm from Ru films on glass, as a function of ruthenium thickness.

Table 1 summarizes the results described above, showing the calculated amounts of absorbed light for 20 nm and 50 nm thick Ru films on glass, sapphire and silicon for a wavelength of 1 000 nm. For each of the three substrates the absolute variation of the amount of absorbed light with film thickness is below 10% for thicknesses above approximately 10 nm.

Table 1. Calculated percentages of absorbed light for 20-nm and 50-nm thick Ru films on different substrates

Substrate	Absorption (20 nm Ru)	Absorption (50 nm Ru)
Glass	34%	30%
Sapphire	32%	30%
Si (includes 5 nm native SiO_2)	24%	29%

As a next step, we tested our patterning method on Ru samples on glass with a thickness of 20 nm and 50 nm, in order to characterize the dependence of the island-formation threshold fluence on film thickness. The samples were exposed to the beam focused to a 2 μm diameter spot, 10 000 pulses and a (single-pulse) fluence varying from 0.8 mJ/cm^2 to 50 mJ/cm^2.

Fig. 3(a) shows the optical microscopy image of an 8×8 grid of Ru/RuO_2 islands remaining after exposure (followed by rinsing in the NaClO solution) of a 20 nm thick Ru film. Each spot corresponds to a different exposure fluence, which increases from the top right to the bottom right corner in a meandering fashion. The first row of islands is missing (top region, hence only 7 rows are visible), and the second row only shows islands, corresponding to the white spots, starting from the second position from the left. The first row is absent because the exposure fluence did not result in the formation of a thick enough oxide to prevent dissolution of the Ru in the NaClO solution. The second line (the first visible one from the top) consists of seven bright spots, corresponding to the Ru/RuO_2 islands. As demonstrated in our previous work [9], the islands can have diameters from 500 nm to a maximum of 2 μm. The exposure fluence for these spots is between 7.8 mJ/cm^2 and 10.25 mJ/cm^2. The regions exposed to higher fluences have an irregular shape and a hole in the center, indicating damage in the form of ablation of the Ru. The same experiment was performed on a 50 nm thick Ru sample, for which we found that the fluence interval corresponding to island formation is from 16.4 mJ/cm^2 to 23.4 mJ/cm^2.

To extract a more precise threshold fluence for island formation, we performed a Liu analysis on the Ru/RuO_2 islands shown in Fig. 3(a) (20 nm thick Ru film), and on the islands obtained on the 50 nm thick Ru sample. The results are shown in Fig. 3(b). For this plot, and for all the others presented in this paper, we only extracted the areas of the "smooth-looking" Ru/RuO_2 islands and excluded the damaged ones. The solid lines are the linear fits to the data, from which

Optical Materials EXPRESS

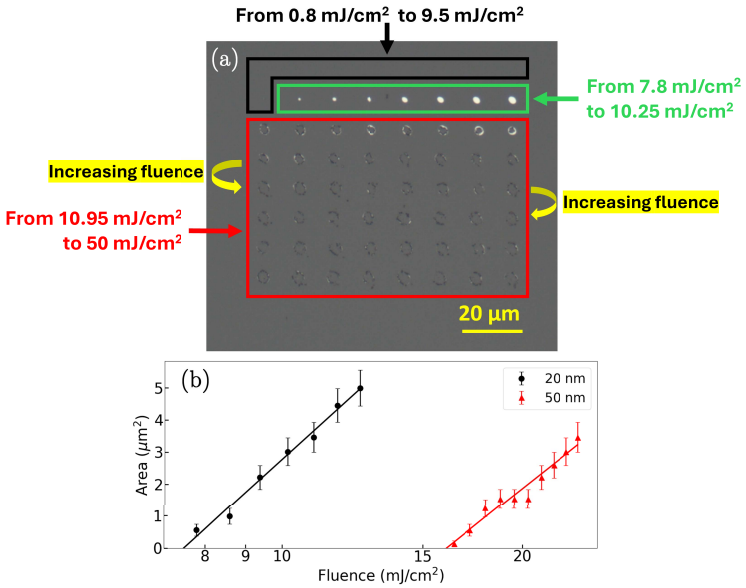

Fig. 3. **(a)** Optical microscopy image of an 8×8 grid of exposure sites obtained from a 20 nm thick Ru film on glass. Each site was exposed to 10 000 pulses with a different fluence, increasing from the top-right to the bottom-right corner of the image (as highlighted by the yellow arrows). The black box highlights the region of the sample in which no Ru/RuO_2 island were found, the green box highlights the islands considered for the analysis of figure (b) and the red one the ablated spots. The boxes are labeled according to the relative exposure fluence ranges.

the threshold fluences are extracted. The island-formation threshold fluence is 7.5 mJ/cm^2 for a 20 nm film, and 16.1 mJ/cm^2 for a 50 nm film. Island formation therefore occurs at a lower fluence for a 20 nm film, compared to a 50 nm one.

Similar results were obtained for the same film thicknesses when exposing the samples to 50 000 pulses, instead of 10 000. In that case, the extracted threshold fluences are 4.8 mJ/cm^2 (for the 20 nm thick film) and 10.8 mJ/cm^2 (for the 50 nm thick film). This agrees with what we have shown earlier [9]: exposure to a higher number of pulses results in only a moderate decrease in the threshold fluence [9]. We note that the ratio between the threshold fluences for the 20 nm film and for the 50 nm one (0.43 for 10 000 pulses exposure; 0.44 for 50 000 pulses exposure) is similar to the ratio of the film thicknesses (0.4). As we show in Fig. 2, the two films absorb similar amounts of light. After absorption, thermalisation of the electrons with the lattice occurs on a picosecond time-scale [14]. After that, the thermal energy density in the film formed at the island formation threshold fluence scales by the same factor as the thickness: an n-fold thickness increase in thickness corresponds to an n-fold increase in threshold fluence. This should allow to extrapolate the fluences necessary to obtain Ru/RuO_2 patterns from Ru films with a chosen thickness, at least as long as it can be assumed that the film is homogeneously heated throughout its thickness. The latter is confirmed by two-temperature model calculations (see also below) for a 50 nm thick layer, which show that after approximately 2.5 ps, the lattice temperature at the surface is only about 20 K higher than at the back of the layer. This might, however, not be true for much thicker films.

In the following, the effect of different substrates on the production of Ru/RuO_2 patterns is studied. We deposited 50-nm-thick Ru films on two additional different substrates: sapphire and silicon. The laser was again focused to a 2 μm spot and the films were exposed to 25 000 pulses.

Optical Materials EXPRESS

The exposure fluence was varied between 0.6 mJ/cm^2 and 40 mJ/cm^2, in an experiment similar to the one resulting in Fig. 3. For sapphire (silicon), Ru/RuO_2 islands are formed for fluences between 15 mJ/cm^2 (15.6 mJ/cm^2) and 29 mJ/cm^2 (30 mJ/cm^2). At higher fluences, damage was observed.

The Liu plots obtained from the optical microscopy images of the samples are shown in Fig. 4. For Ru deposited both on silicon (black dots) and sapphire (red triangles) we observe a linear dependence of the island area on the logarithm of the exposure fluence. This allowed us to perform a linear fit (solid lines) and extract the threshold fluences for island formation, similar to what we did for Ru on glass shown in Fig. 3(b). The threshold fluence is 14.4 mJ/cm^2 for Ru on sapphire and 15.3 mJ/cm^2 for Ru on silicon.

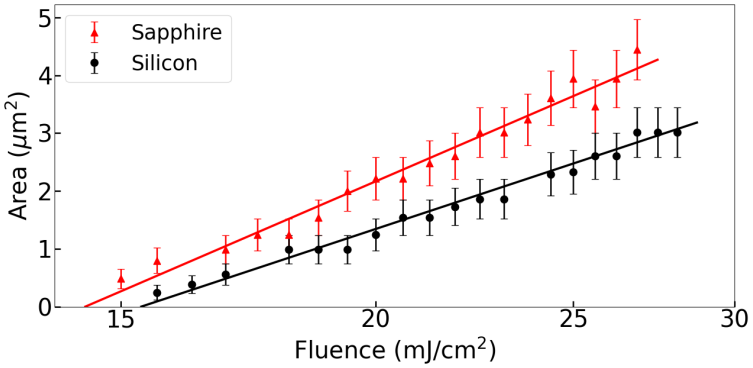

Fig. 4. Liu plots obtained from the areas of Ru/RuO_2 islands produced from 50 nm thick Ru deposited on silicon (black circles) and sapphire (red triangles) exposing the samples to 25 000 pulses

The thermal conductivity of sapphire is 23 W K^{-1} m^{-1} [15], while that of silicon is 142 W K^{-1} m^{-1}. Given such a large difference in the thermal conductivities of the substrates, it is a bit surprising that the threshold fluences for island formation are not very different between sapphire and silicon. Note that these numbers are still comparable with that found for Ru on glass for 10 000 shots (16.1 mJ/cm^2) and for 50 000 shots (10.8 mJ/cm^2), even though glass has a much lower thermal conductivity of about 1.14 W K^{-1} m^{-1}. A higher thermal conductivity should result in a more efficient diffusion of heat from the metal into the substrate, therefore lowering the Ru temperature in a shorter time. This would require higher fluences to maintain a high enough temperature for a long enough time to form the oxide layer which prevents dissolution in the NaClO solution. However, the threshold fluences for Ru on sapphire and on silicon, for example, are very similar (14.4 mJ/cm^2 for Ru on sapphire; 15.3 for Ru on silicon) while their thermal conductivities are very different. The small difference with glass is even more striking, considering that its thermal conductivity is more than an order of magnitude lower than that of sapphire. The fairly similar fluence thresholds are probably due to the presence of a finite heat diffusion-limiting interfacial thermal conductivity (ITC) [14]. Although the quality of the interface was not inspected, we note that the ITC is also affected by deposition defects or roughness at the metal-substrate interface [16], which might be the ultimate factor hindering the heat exchange between the two materials. It is therefore possible that finite ITCs result in similar heat transfer dynamics even if the thermal conductivities of the substrates are largely different. According to this interpretation, the finite ITC acts as a thermally insulating layer limited the heat-transfer. For silicon, the presence of a native oxide may also have an effect on the heat diffusion into the substrate, having interfaces with both the Ru and the silicon, effectively lowering the ITC between the Ru and the silicon.

Optical Materials EXPRESS

The patterning method allows us to fabricate Ru/RuO_2 islands with a diameter below the optical diffraction limit of the system used for the exposure. Indeed, we obtained islands with a diameter of about 500 nm by focusing the 1030 nm laser to a spot with a 2 μm diameter [9]. To study the effect of the laser spot size on the formation of these islands, we exposed the Ru to a beam focused to 0.8 μm diameter. This was done on a 50 nm thick Ru film on glass. Again, 8×8 grids of regions exposed to different fluences were produced.

Fig. 5 is the optical microscopy image of one grid of Ru/RuO_2 islands on glass obtained by exposing the sample to 10 000 laser pulses with a 0.8 μm diameter beam. Similar to Fig. 3(a), the exposure fluence increases from the top-right corner to the bottom-right corner in a meandering way. The exposure fluence was varied between 2 mJ/cm^2 and 124 mJ/cm^2. The two topmost rows of exposed spots are empty, showing that a not thick enough RuO_2 layer formed on top of the Ru, while the islands in the two lowest rows show evident signs of laser-induced damage. This is also true for the five islands on the right of the third row from the bottom of the grid. From this, the fluence resulting in island formation ranges from 35 mJ/cm^2 to 75 mJ/cm^2. This result demonstrates that not only a 2 μm, but also a 0.8 μm dameter exposure spot is capable of producing Ru/RuO_2 islands. Note that because the substrate used for these experiments is glass, SEM imaging could not be used to determine the size of the smallest islands created due to charge accumulation on the sample.

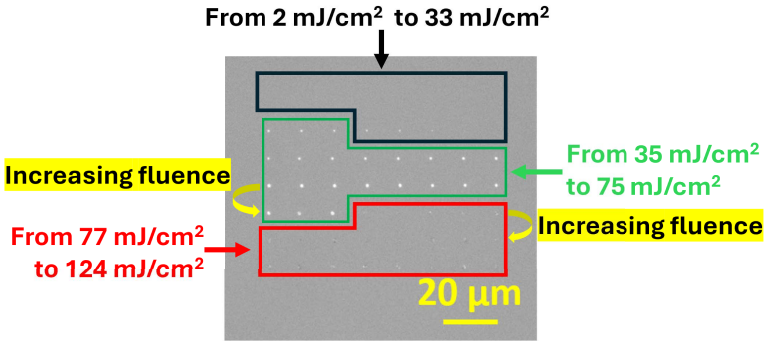

Fig. 5. Optical microscopy image of a grid of Ru/RuO_2 islands obtained with a 0.8 μm exposure diameter. The 50 nm thick Ru film was deposited on glass and exposed to 10 000 pulses with fluence increasing in a meandering fashion. The fluence increases from the top-right to the bottom-right corner of the grid (as highlighted by the yellow arrows). The black box highlights the region of the sample in which no Ru/RuO_2 island was found, the green box highlights the islands considered for the analysis of Fig. 6 and the red one the ablated spots. The boxes are labeled according to the relative exposure fluence ranges.

We repeated the experiment resulting in Fig. 5 by using 1, 1 000, 20 000, 50 000 and 200 000 pulses. Exposure to a single pulse did not result in island formation. The diameters of the Ru/RuO_2 islands on glass were extracted to obtain the Liu plots similar to those of Fig. 3(b), which are shown in Figs. 6(a) to (e).

The corresponding Liu plots are shown in Figs. 6(a)-(e). We note that the islands have dimensions which are close to the resolution of the optical microscope, resulting in the relatively large error bars in the plots. In addition, the smallest increase in island diameter that we could extract corresponds to about one image pixel. For this reason, plateaus appear in the data in the Liu plots. However, it can be seen that the area of the islands scales approximately linearly with the logarithm of the exposure fluence within the error bars, and taking into account the aforementioned step-wise increase due to the microscope resolution. In addition, by comparing Figs. 6(a) to (d), the lowest fluence that results in the formation of a Ru/RuO_2 island decreases with exposure to a higher number of pulses. An exception is Fig. 6(e), corresponding to exposure

Optical Materials EXPRESS

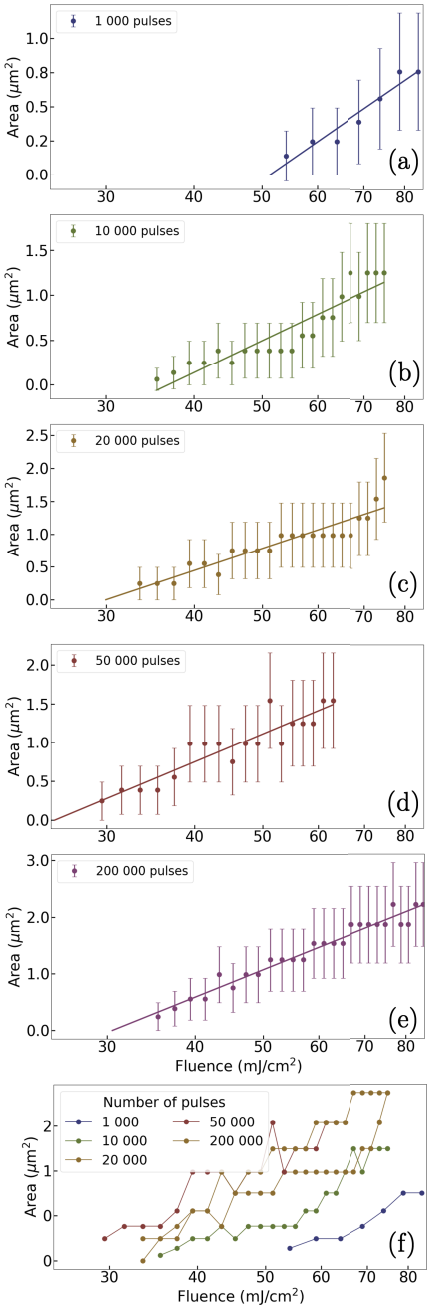

Fig. 6. **(a)**-**(e)** Liu plots obtained by extracting the Ru/RuO_2 island areas after exposure to the laser focused to a 0.8 μm diameter spot, for different numbers of pulses (indicated in the figures). The samples consisted of 50-nm-thick Ru films deposited on glass. **(f)** A single plot showing the curves of figures (a)-(e). The error bars are omitted to facilitate comparison between the curves.

Optical Materials EXPRESS

to 200 000 pulses, in which the smallest island forms at an exposure fluence slightly higher than the one corresponding to 50 000 pulses. This difference is currently not understood. Figure 6(f) shows the curves of Figs. 6(a)-(e) in one single plot, to facilitate their comparison.

To determine the threshold fluence F_0 for island formation, linear fits in the data in Figs. 6(a)-(e) were performed (solid lines), similar to what was done in Figs. 3 and 4. In Fig. 7 we plot F_0 as a function of the number of pulses extracted from the Liu plots of Figs. 6(a)-(e). The threshold fluence decreases steeply in a non-linear fashion from 51 mJ/cm^2 at 1 000 pulses down to 25 mJ/cm^2 at 50 000 pulses. A moderate increase occurs for exposure to 200 000 pulses, at which F_0 has a value of 30 mJ/cm^2. This marked dependence on number of pulses is an indication that heat and/or oxidation accumulation plays a role in the island formation. We note that we can not rule out that the repeated heating and cooling of the layer may lead to material fatigue, which may be (partly) responsible for the observed dependence of the threshold fluence on the number of laser pulses. It is an interesting possibility and may be a topic for further studies.

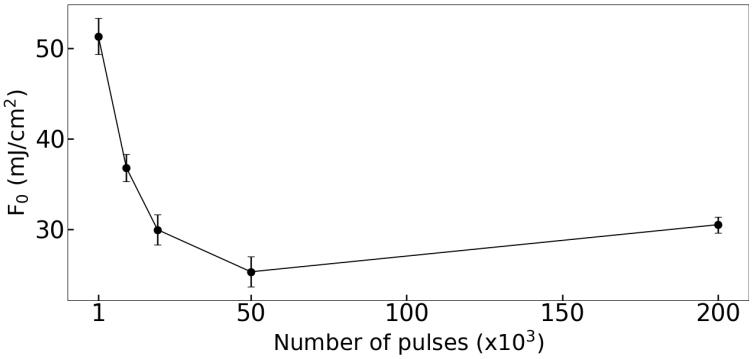

Fig. 7. Island formation threshold fluence F_0 extracted from the Liu plots of Fig. 6 as a function of the exposure number of pulses. The samples consisted of 50-nm-thick Ru films deposited on glass.

In the previous sections, the results obtained by exposing the samples to a beam focused to a 2 μm and to a 0.8 μm diameter were reported. For the 2 μm spot, we found a threshold of 10.8 mJ/cm^2 for Ru on glass exposed to 50 000 pulses, significantly lower than for the 0.8 μm laser spot size.

In order to inspect the morphology of the islands, we performed scanning electron microscopy (SEM) on islands obtained from a 50 nm thick Ru film deposited on silicon and exposed to 1 000 pulses. The laser was focused to a spot with a 2 μm diameter. Figure 8(a) is the SEM image of a region exposed to 21 mJ/cm^2, which is slightly below the island-formation fluence threshold (23 mJ/cm^2). The exposed region shows nearly circular, irregular "porous" film. We interpret this as an incomplete RuO_2 layer on Ru, where the RuO_2 is not thick enough, or too porous, to prevent dissolution of the underlying Ru in the NaClO solution. The film becomes more dense/uniform towards the center of the exposure region, probably due to the higher local intensity in the center of the gaussian beam, resulting in increased oxidation. Figure 8(b) is the SEM image of a spot exposed to a fluence of 30 mJ/cm^2, above the island-formation threshold. In this case, the island has a regular, more smooth morphology, indicating the formation of a thick-enough oxide layer to prevent the NaClO from dissolving the underlying Ru. Similar images did not show significant differences in the morphology of the islands between samples exposed to pulses ranging from 1 000 to 50 000. We did not perform SEM imaging on samples exposed to 200 000 pulses. This means that we can not exclude that a change in morphology due to exposure to such a high number of pulses may be responsible for the increase of F_0 observed for 200 000 pulses (Fig. 7).

Optical Materials EXPRESS

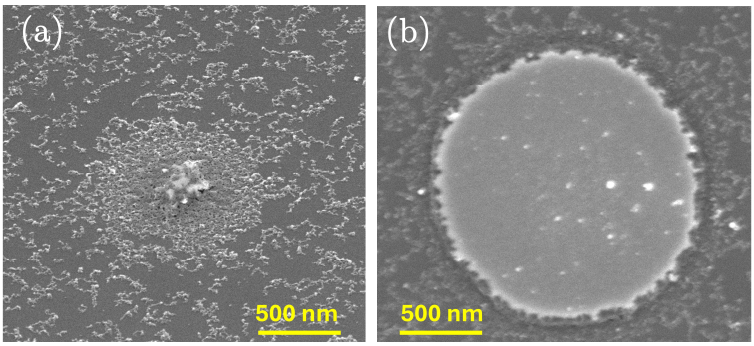

Fig. 8. **(a)** SEM image of a region of a 50 nm thick Ru sample exposed to a fluence slightly below the island-formation threshold fluence (21 mJ/cm^2). **(b)** SEM image of a Ru/RuO_2 island obtained after exposure to a fluence (30 mJ/cm^2) above the island-formation threshold fluence. In both cases ((a) and (b)) the Ru film was deposited on silicon, exposed to 1 000 pulses and the exposure laser was focused to a spot with a diameter of 2 μm.

We now turn to the heat diffusion analysis. Heat deposited by the laser can diffuse in the direction orthogonal to the sample surface and into the substrate, and it can diffuse radially in the in-plane direction. To quantify the effect of heat diffusion, we performed heat diffusion calculations for a 50 nm thick Ru film on glass in order to model the temporal and spatial evolution of the temperature at the surface of the Ru film which, in turn, results in oxidation. In the following, the procedure used for performing these calculations is described.

As a starting point, the percentage of absorbed light was calculated in the same way as for Fig. 2. In metals, the energy deposited by laser illumination is absorbed by the electron gas. The electron gas thermalizes on a timescale of a few hundreds femtoseconds [17]. Subsequently, within a few picoseconds, the electron gas transfers energy to the lattice via electron-phonon coupling. The energy exchange between the electron gas and the lattice is described by the *two-temperature model* (TTM) [18]. This model consists of two coupled differential equations describing the spatio-temporal evolution of the temperature of the electron gas and of the lattice, respectively. The TTM was used to obtain the spatial temperature profile of the lattice once it approximately reaches thermal equilibrium with the electron gas, which occurs after approximately 2 ps after the light absorption. The temperature distribution of the lattice at this moment is used as the starting condition for the single-temperature heat diffusion calculation described below. The latter calculations focus only on the lattice temperature.

In order to model heat transport, we assume rotational symmetry, assuming no azimuthal-angle dependence. The heat diffusion equation thus obtained is:

$$\frac{\partial u}{\partial t} = \frac{k}{\rho c}\left[\frac{\partial^2 u}{\partial r^2} + \frac{1}{r}\frac{\partial u}{\partial r}\right] + \frac{1}{\rho c}\frac{\partial k}{\partial z}\frac{\partial u}{\partial z} + \frac{k}{\rho c}\frac{\partial^2 u}{\partial z^2} \tag{1}$$

where u is the temperature, r is the radial coordinate, z is the depth within the sample, k is the thermal conductivity, ρ the material density and c the specific heat capacity. In-plane heat diffusion is described by the terms between the square brackets. The z-dependence of the thermal conductivity ($k = k(z)$) is included to model a system consisting of different layers. Its derivative is nonzero only at the interface between two materials which, in the case described here, is the interface between the Ru film and the substrate. Equation (1) was numerically solved using a forward-difference method. At the interface between the Ru and the substrate, *jump matching conditions*, as described in [19], were used. Our numerical calculations are limited to single pulse excitation only. Nevertheless, as we will show, this still gives significant insights into the heat diffusion dynamics occurring in our samples.

Optical Materials EXPRESS

The temperature at the surface ($z = 0$) of a 50 nm Ru film on glass was calculated using the method described above, after exposure to a single laser pulse with a gaussian spatial cross section. In the calculations for Ru we used $\rho = 12.45 \times 10^3$kg m^{-3}, $c = 238$ J kg^{-1} K^{-1} and $k = 120$ W K^{-1} m^{-1} [20]. For borosilicate glass we used k = 1.14 W K^{-1}m^{-1}, $\rho = 2.23\times10^3$ kg m^{-3}, and c = 820 J kg^{-1} K^{-1}. The value of the ITC between Ru and glass is unfortunately unknown. A value of 3.5 $\times10^8$ W K^{-1} m^{-2} was measured in [14] for Ru on sapphire. Since we do not know this value for Ru on glass and, furthermore, because it can change based on the Ru deposition method, we varied its value between 10^8 and 10^{10} W m^{-2} K^{-1}. The calculations were performed for exposure diameters of 2 μm and of 0.8 μm. An exposure fluence of 1 nJ was used for the 2 μm diameter beam and 0.16 nJ for the 0.8 μm diameter one. Although heat transport can be affected by differences in the ITC, we found that the general conclusions that we can draw by comparing the results for the two exposure diameters, do not strongly depend on this value.

Fig. 9 shows the temporal evolution of the temperature at the center of a spot exposed to a 2 μm beam diameter (red curve) and to a 0.8 μm beam (black curve). An ITC value of 10^9 W m^{-2} K^{-1} was used in this calculation. From the initial temperature of approximately 935 K, a steep temperature decrease occurs up to approximately 20 ps for both curves, although the decay of the black (dashed) curve begins to deviate from the red (solid) one already around 20 ps. This initial steep decay is associated, in both cases, with the equilibration of the lattice temperature within the Ru layer, as confirmed by comparing these heat transport calculations with TTM calculations in Ru for the first 20 ps. In this time interval, the curves overlap because there has not been enough time yet for radial heat diffusion and heat diffusion into the substrate.

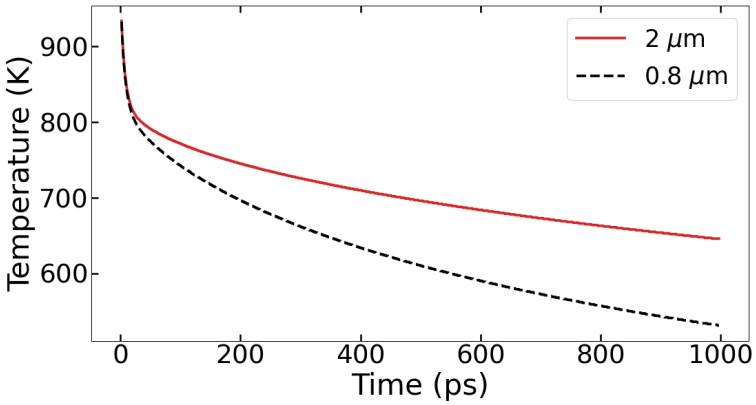

Fig. 9. Calculated temporal evolution of the surface temperature at the center of the illuminated spot on a 50 nm thick Ru film on glass for a 2 μm (red) and a 0.8 μm (black dashed) beam diameter.

The faster decay of the surface temperature observed at times >20 ps for the 0.8 μm diameter exposure with respect to that of the 2 μm exposure is due to the fact that, for a smaller focal diameter, the spatial temperature distribution has a steeper gradient in the radial direction. For Ru, for spot sizes smaller than about 1 μm diameter, loss of heat in the center of the spot due to radial heat diffusion overtakes loss of heat by diffusion into the substrate. This results in a more rapid in-plane heat transport and, therefore, more rapid temperature decrease. or the calculations described above we did not consider the temperature decrease occurring via emission of thermal radiation. We estimated that the amount of energy lost via this process on a scale of 5 μs, the time interval between subsequent pulses, is negligible compared to the one lost via heat diffusion. Details on the calculations can be found in the Supplement 1.

Optical Materials EXPRESS

4. Discussion

The partial oxidation of the Ru film, which prevents dissolution of the exposed regions in the NaClO solution, occurs as a consequence of a laser-induced temperature increase of the metal. A thick enough oxide is formed once a high enough temperature is reached and maintained for a long enough time. Testing the Ru/RuO_2 formation method on Ru films with different thicknesses and on films deposited on different substrates provides insight into the role of heat diffusion orthogonal to the sample surface. In particular, the results presented in Figs. 3 indicate that the threshold fluence necessary for the formation of a thick enough RuO_2 layer (F_0) depends directly on the initial Ru thickness. This result, combined with the fact that the calculated optical properties of Ru showed a moderate dependence on the film thickness between ~ 8 nm and 100 nm (Fig. 2), strongly suggests that the threshold fluence for Ru/RuO_2 island formation in these samples solely depends on the energy density in the film after exposure. This conclusion holds as long as the Ru film is homogeneously heated over its thickness. For much thicker films this consideration probably does not hold. However, within the limit of homogeneously heated films, once F_0 has been determined for the exposure conditions used, such as the number of pulses or the beam diameter, it is possible to estimate a priori the value of F_0 for a different film thickness.

The observation of similar island-formation threshold fluences obtained for Ru deposited on substrates with a relatively large difference in thermal conductivities (sapphire, silicon and glass) can be explained in terms of the interfacial thermal conductance between the metal and the substrate. For a homogeneously heated Ru film the lattice temperature decreases as a consequence of in-plane heat transport and diffusion into the substrate. Ideally, if the ITC between the metal and the substrate was infinite, heat diffusion from the Ru into the substrate would be purely determined by the thermal conductivity and the heat capacity of the substrate, as well as the total thermal energy contained in the Ru, and so would the threshold fluence F_0. However, finite values of ITC limit the heat diffusion from the metal into the substrate. It is therefore possible that differences in the thermal conductivities of the substrates are compensated by differences in the ITC, resulting in similar threshold fluences. This hypothesis should be confirmed by measurements of the ITC, which unfortunately are non-trivial to do and which were not performed at this stage.

We note that, between 300 K and 1000 K, thermal conductivities for both silicon and sapphire decrease by about a factor five [21,22]. This temperature dependence of the thermal conductivity is not included in the calculations. However, even if we were to include this, it would not explain the comparable oxidation fluence thresholds observed in all three materials. For lack of a better explanation, we therefore think that a finite interfacial thermal conductance (ITC) is the most likely explanation. Such an interface thermal conductance may also be influenced by the morphology of the Ru/substrate interface, about which we currently have no information.

The role of in-plane heat diffusion is understood as follows. Figure 7 shows a steep non-linear decrease of F_0 obtained after exposure to an increasing number of pulses using a 0.8 μm beam diameter. This result differs from our previous observation of a moderate linear decrease obtained when using a 2 μm exposure diameter [9]. The calculated temporal evolution of the Ru lattice-temperature at the surface of the film shows a faster temperature decay after exposure to the 0.8 μm beam starting from approximately 20 ps after exposure. This is due to the fact that the smaller exposure spot corresponds to a steeper radial temperature gradient. This increases the rate of in-plane heat diffusion and results in a faster temperature decay. For this reason, the decrease of the surface temperature at the center of the exposed region during the 5 μs occurring between the arrival of each laser pulse (since the repetition rate of the laser is 200 kHz) is significantly larger for exposure to the 0.8 μm beam than for the 2 μm one. The key difference here is that, after exposure to a 2 μm spot, a high enough temperature necessary for oxidation is maintained for a long enough time, allowing oxidation of a small fraction of the film. For the 0.8 μm beam and the same number of laser exposure pulses, on the other hand, the thermal decay is

Optical Materials EXPRESS

faster. Therefore, a higher initial temperature needs to be reached and thus a higher fluence has to be used so that the surface lattice temperature is maintained above the oxidation threshold temperature for a long enough time after exposure. The latter conclusion is also supported by the fact that, overall, the threshold fluences extracted for exposure to the 0.8 μm exposure diameter are higher than those extracted for the 2 μm exposure.

A potentially limiting factor for the spatial resolution of our patterning process might be oxygen diffusion. However, as we mentioned above and in our previous publication [9], the oxide layer is approximately 2 nm thick. This suggests a slow diffusion of oxygen along the direction orthogonal to the sample surface, resulting in the formation of a thin oxide layer. If we assume that the in-plane oxygen diffusion occurs on a similar length scale, a negligible effect on spatial resolution and processing time is expected. In addition, the fact that we could obtain islands with a diameter four times smaller than the laser exposure diameter rules out a significantly large effects. Details about oxygen diffusion in Ru oxidation can be found elsewhere [23].

5. Conclusion

We have studied the formation of Ru/RuO_2 islands on various substrates, formed by partial oxidation of the Ru by multiple focused laser pulses, followed by removal of the unoxidized Ru in a NaClO solution. From measurements on 20- and 50-nm-thick Ru layers on glass, and from the calculated amount of absorbed light, we conclude that the fluence threshold for island formation can be estimated a priori for different layer thicknesses. Subsequently, the role of the substrate material was tested leading to the conclusion that the main parameter determining the island-formation threshold fluence for different substrate materials is the interfacial thermal conductance between the Ru and the substrate, rather than the thermal conductivity of the substrate alone.

When using a sub-micron exposure beam diameter we also show that in-plane heat diffusion likely affects the island-formation process. Although a small exposure diameter may make it possible to produce patterns with increasingly small dimensions, we show that the role of in-plane heat diffusion must be taken into account as it may limit the effective spatial resolution achievable by this patterning method.

Acknowledgments. This work was partly conducted at the Advanced Research Center for Nanolithography, a public-private partnership between the University of Amsterdam (UvA), Vrije Universiteit Amsterdam (VU), Rijksuniversiteit Groningen (RUG), the Netherlands Organization for Scientific Research (NWO), and the semiconductor equipment manufacturer ASML. Marnix Vreugdenhil acknowledges the financial support by the project "Wafer damage control: Understanding and preventing light-induced material changes in optical measurement systems" (with Project No. 17963) of the research program High Tech Systems and Materials (HTSM), which is (partly) financed by the NWO.

Disclosures. The authors have no conflicts to disclose.

Data availability. Data underlying the results presented in this paper are not publicly available at this time but may be obtained from the authors upon reasonable request.

Supplemental document. See Supplement 1 for supporting content.

References

1. D. Choi and K. Barmak, "On the potential of tungsten as next-generation semiconductor interconnects," Electron. Mater. Lett. **13**(5), 449–456 (2017).
2. J. H. Moon, E. Jeong, S. Kim, *et al.*, "Materials quest for advanced interconnect metallization in integrated circuits," Adv. Sci. **10**(23), 2207321 (2023).
3. E. Milosevic, S. Kerdsongpanya, A. Zangiabadi, *et al.*, "Resistivity size effect in epitaxial Ru(0001) layers," J. Appl. Phys. **124**(16), 165105 (2018).
4. L. G. Wen, P. Roussel, O. V. Pedreira, *et al.*, "Atomic layer deposition of ruthenium with tin interface for sub-10 nm advanced interconnects beyond copper," ACS Appl. Mater. Interfaces **8**(39), 26119–26125 (2016).
5. S. Gupta, M. Sinha, R. Dhawan, *et al.*, "Study of oxidation behaviour of ruthenium thin film after thermal annealing in oxygen environment," Thin Solid Films **764**, 139606 (2023).
6. H.-C. Wen, P. Lysaght, H. N. Alshareef, *et al.*, "Thermal response of Ru electrodes in contact with SiO2 and Hf-based high-k gate dielectrics," J. Appl. Phys. **98**(4), 043520 (2005).

Optical Materials EXPRESS

7. S. Yulin, N. Benoit, T. Feigl, *et al.*, "Mo/Si multilayers with enhanced TiO_2- and RuO_2-capping layers," in *Emerging Lithographic Technologies XII*, vol. 6921 F. M. Schellenberg, eds., International Society for Optics and Photonics (SPIE, 2008), p. 692118
8. G. Miao, A. Gupta, G. Xiao, *et al.*, "Epitaxial growth of ruthenium dioxide films by chemical vapor deposition and its comparison with similarly grown chromium dioxide films," Thin Solid Films **478**(1-2), 159–163 (2005).
9. L. Cruciani, M. Vreugdenhil, S. van Vliet, *et al.*, "Direct laser patterning of ruthenium below the optical diffraction limit," Appl. Phys. Lett. **124**(17), 171902 (2024).
10. M. Vreugdenhil and D. van Oosten, "A highly automated apparatus for ultra-fast laser ablation studies," Rev. Sci. Instrum. **93**(7), 073003 (2022).
11. J. M. Liu, "Simple technique for measurements of pulsed gaussian-beam spot sizes," Opt. Lett. **7**(5), 196–198 (1982).
12. S. Elhadj and J. H. Yoo, "Efficient method for the measurement of lifetime optical damage performance of thin film coatings from laser damage size analysis," Opt. Lett. **42**(16), 3153–3156 (2017).
13. G. de Haan, T. J. van den Hooven, and P. C. M. Planken, "Ultrafast laser-induced strain waves in thin ruthenium layers," Opt. Express **29**(20), 32051–32067 (2021).
14. H. J. Shin, J.-M. Lee, S. Bae, *et al.*, "Metal-insulator transition and interfacial thermal transport in atomic layer deposited ru nanofilms characterized by ultrafast terahertz spectroscopy," Appl. Surf. Sci. **563**, 150184 (2021).
15. K. A. McCarthy and S. S. Ballard, "New data on the thermal conductivity of optical crystals*," J. Opt. Soc. Am. **41**(12), 1062–1063 (1951).
16. T. Lu, J. Zhou, T. Nakayama, *et al.*, "Interfacial thermal conductance across metal-insulator/semiconductor interfaces due to surface states," Phys. Rev. B **93**(8), 085433 (2016).
17. V. E. Gusev and O. B. Wright, "Ultrafast nonequilibrium dynamics of electrons in metals," Phys. Rev. B **57**(5), 2878–2888 (1998).
18. L. Jiang and H.-L. Tsai, "Improved two-temperature model and its application in ultrashort laser heating of metal films," J. Heat Transfer **127**(10), 1167–1173 (2005).
19. R. Hickson, S. Barry, G. Mercer, *et al.*, "Finite difference schemes for multilayer diffusion," Mathematical and Computer Modelling **54**(1-2), 210–220 (2011).
20. N. Milošević and I. Nikolić, "Thermophysical properties of solid phase ruthenium measured by the pulse calorimetry technique over a wide temperature range," Int. J. Mater. Res. **106**(4), 361–367 (2015).
21. E. R. Dobrovinskaya, L. A. Lytvynov, and V. Pishchik, *Properties of Sapphire* (Springer US, 2009), pp.55–176.
22. C. J. Glassbrenner and G. A. Slack, "Thermal conductivity of silicon and germanium from 3°k to the melting point," Phys. Rev. **134**(4A), A1058–A1069 (1964).
23. R. Coloma Ribera, R. W. E. van de Kruijs, A. E. Yakshin, *et al.*, "Determination of oxygen diffusion kinetics during thin film ruthenium oxidation," J. Appl. Phys. **118**(5), 055303 (2015).